Highly Sensitive Surface Acoustic Wave H$_2$S Gas Sensor Using Electron-beam-evaporated CuO as Sensitive Layer

Lei Zhao,[1†] Jian Che,[2†] Qingqing Cao,[1] Shanshan Shen,[1] and Yongliang Tang[2*]

[1]School of Aeronautic Engineering, Nanjing Vocational University of Industry Technology,
Nanjing 210023, P.R. China
[2]School of Physical Science and Technology, Southwest Jiaotong University, Chengdu 610031, P.R. China

H$_2$S is a crucial industrial gas and also a neurotoxin which poses a significant threat to human life and safety in case of leakage. Therefore, it is essential to monitor the H$_2$S concentration in real time during industrial production and daily life. In this study, we utilized a method that combined electron beam evaporation and annealing to deposit a CuO film on a two-port quartz surface acoustic wave (SAW) resonator, which was connected to peripheral circuits to build a SAW sensor. The sensor exhibited excellent sensitivity, selectivity, and stability, and had a response of −30 kHz to 4 ppm H$_2$S at *RH* = 60% and room temperature. The superior performance is attributed to the strong chemical adsorption of CuO toward H$_2$S. CuO reacts with H$_2$S to form CuS, leading to an increase in the mass of the film, which causes the negative frequency response of the sensor. It is also revealed that environmental humidity has a significant impact on the sensor response, with higher humidity resulting in a stronger response.

1. Introduction

H$_2$S is a highly toxic gas, with toxicity lower than that of cyanide, but five to seven times higher than that of carbon monoxide and sulfur dioxide.[1–3] The lethal concentration of H$_2$S is 500 ppm, and the threshold safe concentration for human beings is limited to lower than 20 ppm. Extremely high concentrations (above 600 ppm) of H$_2$S can cause sudden death, where the person falls to the ground instantly as if electrocuted.[4–6] Despite its high toxicity, people inevitably come into contact with H$_2$S in industrial production processes. For example, H$_2$S is commonly used in the manufacture of fluorescent powders, optical conductors, reducing agents, pesticides, pharmaceuticals, and sulfides.[7–10] H$_2$S is also widely present in oil and gas extraction processes, posing a significant threat.[10] For instance, a blowout accident occurred in Chongqing on December 2003 and caused 243 deaths and 2142 hospitalizations due to H$_2$S poisoning. The accident site failed to detect the concentration of H$_2$S, resulting in the tragedy. Therefore, it is of great importance to perform real-time and rapid detection of H$_2$S to protect

people's lives and ensure property safety in oil and gas fields and some industrial production processes using high-sensitivity H_2S sensors.

After years of exploration, different types of H_2S gas sensor have been developed on the basis of different sensing materials and methods, which can be roughly divided into semiconductor-type, electrochemical-type, optical-type, catalytic combustion-type, and piezoelectric-type sensors.[11–14] Among them, piezoelectric-type surface acoustic wave (SAW) sensors have the advantages of fast response, high precision, low cost, real-time measurement, among others.[14–16] The core component of SAW sensors is a SAW resonator with a sensitive film on its surface. The sensitive film adsorbs H_2S gas in the environment, which causes changes in the physical properties of the films, leading to a variation in the central frequency of the resonators and the responses of the sensors. [15,16]

Recently, some semiconductor oxide materials, such as ZnO, WO_3, Fe_2O_3, SnO_2, and CuO, have been widely used as sensitive films for SAW sensors.[16–22] Among them, CuO has strong adsorption capabilities for H_2S and can further react with H_2S.[15,22] The adsorption and reaction can cause significant changes in mass, elastic modulus, and conductivity of CuO, which leads to frequency responses of the SAW sensors. For example, our previous research has shown that a SAW sensor based on a sol–gel CuO film has a response of −8 kHz to 8 ppm H_2S.[23] However, in most of the previous studies, the sensing mechanism of the SAW H_2S gas sensors based on CuO films has not been fully elucidated Particularly, the contributions of the changes in the film's conductivity, elastic modulus, and mass to the responses of the sensor have not been fully understood.

In this study, we utilized a method that combined electron beam evaporation and annealing to deposit a CuO film on a two-port quartz SAW resonator, which was then connected to peripheral circuits to build a sensitive SAW sensor. The sensor's performance was investigated. The sensing mechanism, especially the contributions of the changes in the film's conductivity, elastic modulus, and mass to the responses of the sensor, was fully revealed.

2. Experimental Details

Two-port SAW resonators [Fig. 1(a) and 1(b)] were used in this work. The length, width, and thickness of the resonator were 13, 2.2, and 0.5 mm, respectively. The specific parameters of the resonator can be found in our previous publication.[15] The transmission characteristics (S_{21}) of the resonator are shown in Fig. 1(c), with a center frequency of ~200 MHz, insertion loss of −10.03 dB, and quality value (Q) of 7758.

Copper (99.99% purity) was used as the target material, and Cu films were deposited on the surface of the SAW resonators and reference Si substrates by electron beam evaporation. During the deposition, the electron beam power upper limit was set to 20%, and the deposition rate was 0.1 Å/s. By adjusting the deposition time, Cu films with thicknesses of 20, 30, 40, and 50 nm were obtained (the thickness was determined using a quartz crystal microbalance). The coated resonators were placed in a muffle furnace and annealed in air at 400 ℃ for 2 h to allow the oxidation of the Cu films. For convenience, the films with different thicknesses were denoted as Cu-20, Cu-30, Cu-40, and Cu-50.
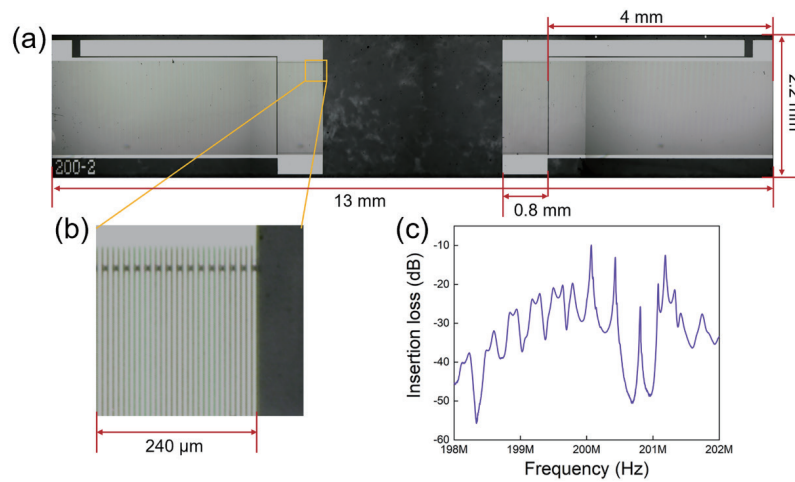
Fig. 1.   (Color online) (a) Optical microscopy image of a SAW resonator. (b) Enlarged picture of the yellow box in (a). (c) Transmission feature (S_{21}) of SAW resonator.

The coated resonator was connected to the peripheral circuit (including amplifier and phase shifter) to form a SAW sensor [Fig. 2(a)]. To accelerate the recovery of the sensor, a Ni-Cr heater was placed under the SAW resonator to heat the film. To conduct the sensing test, the sensor was placed in a 20 L chamber [Fig. 2(b)]. A DC power supply (Agilent) was used to power the sensor. The sensor was then connected to a frequency counter (HP 5385A) for real-time frequency acquisition.

During the test, the temperature and humidity in the chamber were maintained at 25 °C and 60%, respectively, unless otherwise specified. Different amounts of test gases (H_2S, H_2, CO, CH_4, NH_3, NO_2, and CH_3CH_2OH, 2 V% diluted in dry air) were injected into the test chamber using a precision syringe to obtain the response of the sensor to different gases. The response of the sensor was defined as $\Delta f = f_s - f_0$, where f_s is the operating frequency of the sensor in the test gas, and f_0 is the operating frequency of the sensor in the atmospheric environment. After the response ceased, the test gas was evacuated from the test chamber to allow the recovery of the sensor.

In this work, the transmission characteristics of the SAW resonator were measured using a vector network analyzer (Keysight E5071C). The microstructure and elemental composition of the films were analyzed using a field emission scanning electron microscope (SEM, FEI Inspect F) and its affiliated energy dispersive X-ray spectroscopy (EDS). The Raman spectra of the films were obtained using a Raman spectrometer (WITec Alpha 300). The conductivity of the films was tested using a Keithley 2400 digital source meter.

3.   Results and Discussion

SEM images of CuO films with different thicknesses are shown in Fig. 3. It can be seen that all the films have relatively dense surfaces. As the film thickness increases, the average particle size on the film surface increases from 24.4 to 60.9 nm, and the surface becomes rougher. For
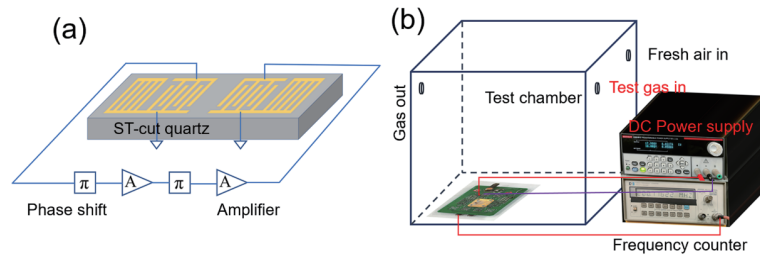
Fig. 2.   (Color online) (a) Schematic diagram of a SAW sensor. (b) Test setup.
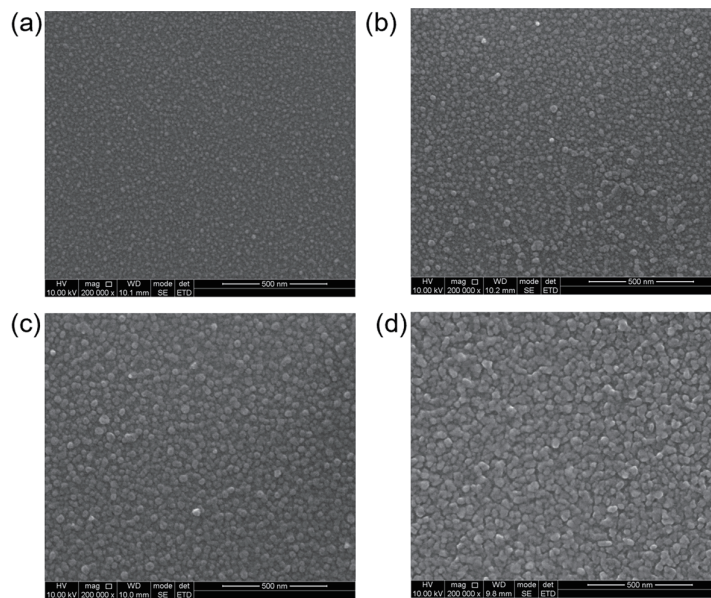
Fig. 3.   SEM images of (a) Cu-20, (b) Cu-30, (c) Cu-40, and (d) Cu-50.

the dense sensitive film, gas may mainly adsorb on the surface of the film. Therefore, the rougher surface may lead to more gas adsorption sites, which results in the stronger response of the sensor.

Figure 4 shows EDS spectra of CuO films with different thicknesses coated on the reference Si substrates before and after coming into contact with H_2S. In all the spectra, a sharp Si peak can be observed, which is caused by the silicon substrate. Before the film comes into contact with H_2S, peaks of Cu and O appear in the spectra, indicating that the film is CuO. In addition, as the film thickness increases, the Cu and O peaks in the spectra become stronger, indicating that the content of CuO on the substrate surface is increasing. After the film comes into contact with H_2S, the intensity of the O peak decreases, and an S peak appears. This indicates that CuO reacts with H_2S and generates CuS or Cu_2S. In addition, the content of S also increases with increasing film thickness, indicating that more H_2S can be adsorbed on the thicker film, leading to more CuS or Cu_2S generated. This may result in the stronger response of the sensor, which is consistent with the SEM result.
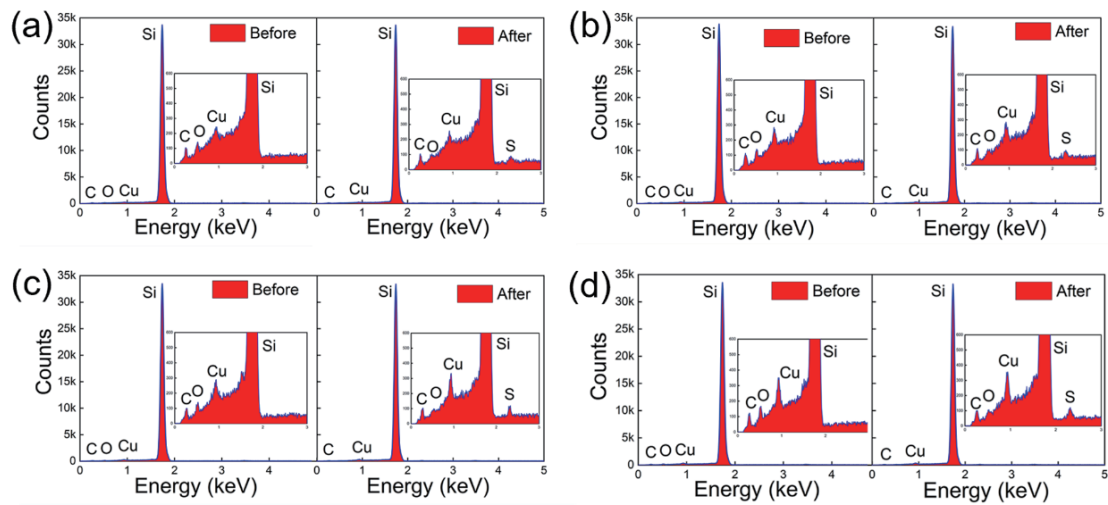
Fig. 4.   (Color online) EDS spectra of (a) Cu-20, (b) Cu-30, (c) Cu-40, and (d) Cu-50 before and after coming into contact with H$_2$S.

The Raman spectra of the Cu-30 film before and after coming into contact with H$_2$S are shown in Fig. 5. All the spectra have a peak at 533 cm^{-1}, which is the Si peak. Before the film comes into contact with H$_2$S, a series of peaks can be observed at 114, 164, 228, 312, and 648 cm^{-1}, which can be attributed to the Ag and B2g Raman vibration modes of CuO.[24–26] This result once again confirms that the film is CuO. After the film comes into contact with H$_2$S, three new peaks appear in the Raman spectra at 122, 277, and 485 cm^{-1}, which are the characteristic peaks of CuS.[27–29] This result further confirms that the CuO film reacts with H$_2$S to generate CuS, which is consistent with the EDS results.

The response of SAW sensors based on CuO films with different thicknesses to 4 ppm H$_2$S is shown in Fig. 6(a). It can be seen that all the sensors have negative frequency responses to H$_2$S, which are −30, −47, −60 and −78 kHz, respectively, and the frequency response is approximately linearly related to the thickness. This result proves the excellent adsorption ability of CuO films to H$_2$S, which is consistent with EDS and Raman results. In addition, the results also show that Cu-50 films with rougher surfaces have more adsorption sites and can adsorb more H$_2$S molecules. After the response process is over, H$_2$S is pumped out of the test chamber to facilitate the recovery of the sensor. However, the experimental results show that all the sensors cannot recover to their initial state, which confirms that CuO reacts with adsorbed H$_2$S to produce CuS following Eq. (1).

$$CuO + H_2S(ads) = CuS + H_2O \tag{1}$$

This reaction has a negative enthalpy, indicating that the reaction between CuO and H$_2$S is an irreversible and exothermic process at room temperature. Therefore, it is difficult for the sensor to recover at room temperature. However, previous studies have revealed that the reaction may
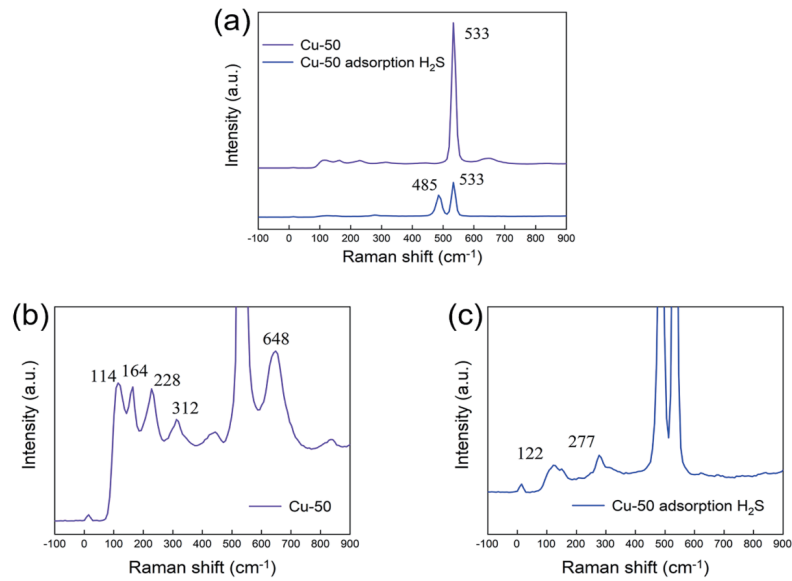
Fig. 5.   (Color online) Raman spectra of Cu-50 film before and after coming into contact with H_2S.
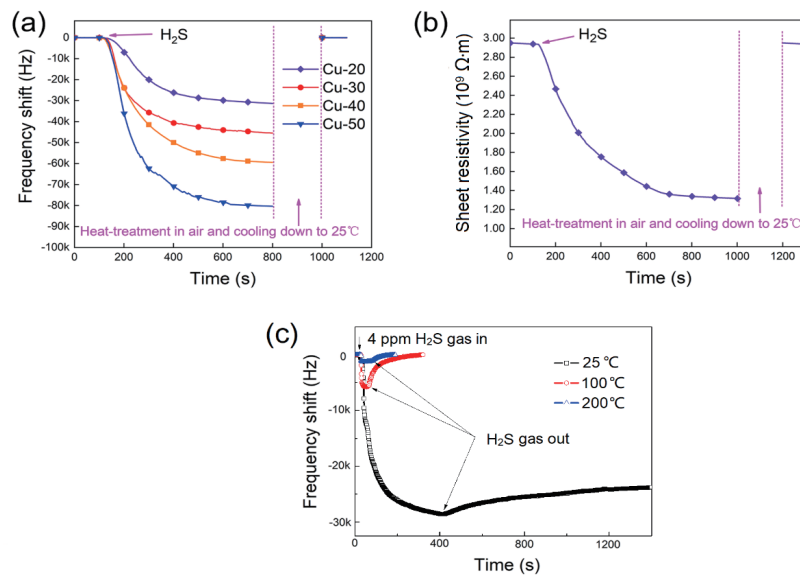
Fig. 6.   (Color online) (a) Dynamic frequency responses of sensors with Cu-20 to Cu-50 to 4 ppm H_2S. (b) Dynamic sheet resistivity of Cu-20 during its contact with 4 ppm H_2S. (c) Dynamic frequency responses of sensors with Cu-20 toward 4 ppm H_2S under 25, 100 and 200 °C.

become reversible when the sensing temperature is increased to 200 °C or higher. Therefore, to promote the recovery of the sensor, namely to promote CuS to be oxidized to CuO, the sensitive film is heated to 200 °C for 2 min to accelerate the oxidation of CuS. After that, the film is allowed to cool naturally to room temperature. By this method, the sensor can quickly recover to its initial state.

The working temperature also affects the response process. Therefore, the Cu-20 sensor's dynamic responses toward 4 ppm H_2S at 25, 100 and 200 °C are further evaluated. As shown in Fig. 6(c), the sensor shows much faster response and recovery at higher operating temperatures. However, the absolute response of the sensor decreases significantly because of the weaker adsorption by H_2S on the film at high temperatures. Therefore, the response process is conducted at room temperature while the recovery is conducted at 200 °C for our sensor to ensure good sensitivity and fast recovery simultaneously.

As shown in Eq. (1), the reaction between the CuO film and adsorbed H_2S produces CuS, which causes the frequency response of the sensor. This reaction may cause three changes in the film, namely, mass change (mass loading effect), elastic modulus change (modulus loading effect), and conductivity change (electrical loading effect), and all three effects may affect the frequency response of the sensor. To investigate the contribution of these three effects to the frequency response, the dynamic change in conductivity of the CuO-20 film during its contact with H_2S was investigated. As shown in Fig. 6(b), when the Cu-20 film comes into contact with H_2S, its sheet resistivity decreases from 2.94×10^9 to 1.32×10^9 $\Omega \cdot m$. Previous studies have revealed that the change in film conductivity affects the frequency response of the sensor according to Eq. (2).[30]

$$\Delta f = -f_0 \times \frac{K^2}{2} \times \Delta \left(\frac{1}{1 + \left(\dfrac{v_0 c_s}{\sigma_s} \right)^2} \right) \tag{2}$$

In Eq. (2), f_0 (=~201 MHz) is the resonant working frequency of the ST-cut quartz SAW resonator, v_0 (=3158 m/s) is the unperturbed SAW velocity on the SAW resonator, K_2 (=0.0011) is the electromechanical coupling coefficient for ST-cut quartz substrate, C_s (=~5.0 × 10⁻¹¹ F/m) is the capacitance of the SAW resonator per unit length, and σ_s is the sheet conductivity of the sensing layer. According to Eq. (2), the theoretical contribution of the change in film conductivity to the frequency response is far less than the measured frequency response. Therefore, it can be concluded that the contribution of the electrical loading effect can be neglected, and the mass loading and modulus loading effects play a major role in the response of the sensor.

CuO reacts with H_2S to generate CuS, which has a greater mass than CuO, so this reaction makes the film heavier. The formation of CuS also leads to a decrease in the film's porosity, resulting in an increase in the film's elastic modulus.[31] The relationships between the change in film mass, elastic modulus, and sensor frequency response are determined using Eq. (3).[32]

$$\Delta f = p\Delta E + (k_1 + k_2) \times f_0^2 \times \Delta m \tag{3}$$

In Eq. (3), p is a positive constant, whereas k_1 and k_2 are negative in sign, and Δm and ΔE are the changes in film mass and elastic modulus, respectively. According to Eq. (3), an increase in film mass results in a negative frequency response of the sensor, whereas an increase in elastic modulus results in a positive frequency response. From Fig. 6(a), it can be seen that all the sensors respond negatively to H_2S; hence, it can be concluded that the mass change, i.e., the mass

loading effect, is the main contributor to the sensor's frequency response. This result is consistent with the SEM result, which shows that the film has a dense structure and that H_2S mainly adsorbs on the surface of the film instead of entering the film, which results in an increase in film mass but little change in elastic modulus.

For practical sensors, the signal-to-noise ratio (defined as the maximum magnitude of the frequency jitter) is a more important parameter than the absolute response. Although the absolute response of the sensor increases with increasing film thickness, the noise also increases due to the larger insertion loss and lower Q value of the SAW resonator for thicker films, as shown in Fig. 7. The noise levels of the four sensors are 9.2, 18.0, 23.8 and 26.3 Hz, and the signal-to-noise ratios are ~3230, 2610, 2520, and 2970, respectively, and the sensor based on the Cu-20 film has the highest signal-to-noise ratio. Therefore, this sensor was selected for further sensing performance evaluation.

Figure 8(a) shows the dynamic responses of the sensor to H_2S in the concentration range from 0.05 to 20 ppm. It can be seen that the sensor's response increases with increasing H_2S concentration. When the concentration is 0.05 and 20 ppm, the response is −9 and −73 kHz, respectively. The noise level of the sensor is 9.2 Hz, so the signal-to-noise ratio is as high as ~978 for 0.05 ppm H_2S, indicating that this sensor may have a lower detection limit (LOD) below 0.05 ppm. However, limited by the experimental facilities, we cannot obtain H_2S at concentration lower than 0.05, so the response toward the H_2S at lower concentration wasn't measured. Furthermore, the reproducibility of the sensor was also investigated by placing it three times in an environment with 4 ppm H_2S. As shown in Fig. 8(b), the sensor's three responses are similar,
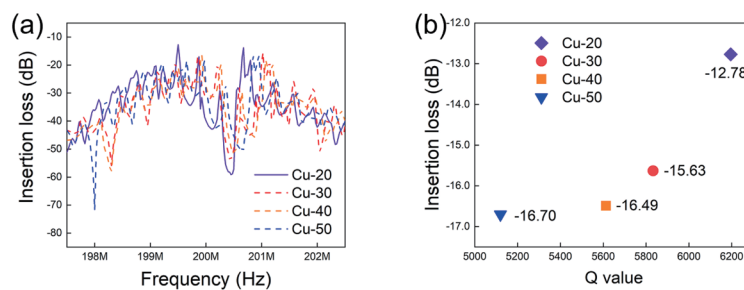
Fig. 7. (Color online) Transmission feature of the SAW resonators with Cu-20 to Cu-50. (b) Insertion loss and Q of SAW resonators with Cu-20 to Cu-50.
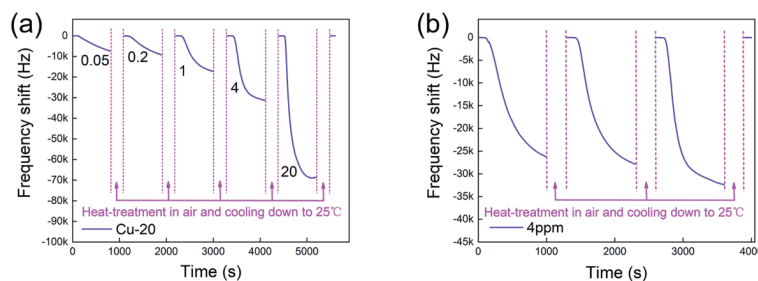
Fig. 8. (Color online) (a) Dynamic responses of sensor with Cu-20 to 0.05−20 ppm H_2S. (b) Dynamic responses of sensor with Cu-20 to 4 ppm H_2S for three consecutive times.

indicating good reproducibility. To evaluate the selectivity, the sensor was put in environments with 50 ppm H_2, CO, CH_4, NO_2, CH_3CH_2OH, and NH_3, and 4 ppm H_2S. As shown in Fig. 9(a) and 9(b), the sensor does not respond to H_2, CO, CH_4, NO_2, or CH_3CH_2OH, and has a response of −2.2 kHz to 50 ppm NH_3. However, this response is much weaker than its response to 4 ppm H_2S, indicating that the sensor also has good selectivity for H_2S. To further evaluate the long-term stability of the sensor, 15 response/recovery cycles were conducted in 15 days. The result is shown in Fig. 9(c) and indicates that the sensor's response toward 0.2, 4 and 20 ppm H_2S is similar for 15 cycles. Therefore, it can be concluded that the sensor has an excellent long-term stability, and the degradation of the sensor's electrodes never occurred in our test process.

Humidity has a strong effect on the sensing performance. Therefore, the sensing performance of the sensor under different humidity conditions was investigated. As shown in Fig. 10(a), when the ambient humidity changes from 50 to 60%, the sensitive film adsorbs more water molecules, resulting in an increase in the mass of the film, and the sensor's frequency baseline decreases by −1.8 kHz. Furthermore, when the ambient humidity changes from 60 to 70%, the baseline decreases by −6.7 kHz. At different humidity levels, the sensor responds to 4 ppm H_2S at −20, −32, and −82 kHz. This indicates that water molecules enhance the adsorption and reaction of CuO to H_2S, which is consistent with previous reports. Nevertheless, although the sensor has a stronger absolute response to H_2S under higher humidity, the noise of the sensor also increases, and the signal-to-noise ratio decreases, as shown in Fig. 10(b). Therefore, the optimal operating humidity for the sensor is $RH = 60\%$. Figures 10(c) and 10(d) show that the insertion loss of the SAW resonator increases with the RH value, which causes the increase in the noise level.
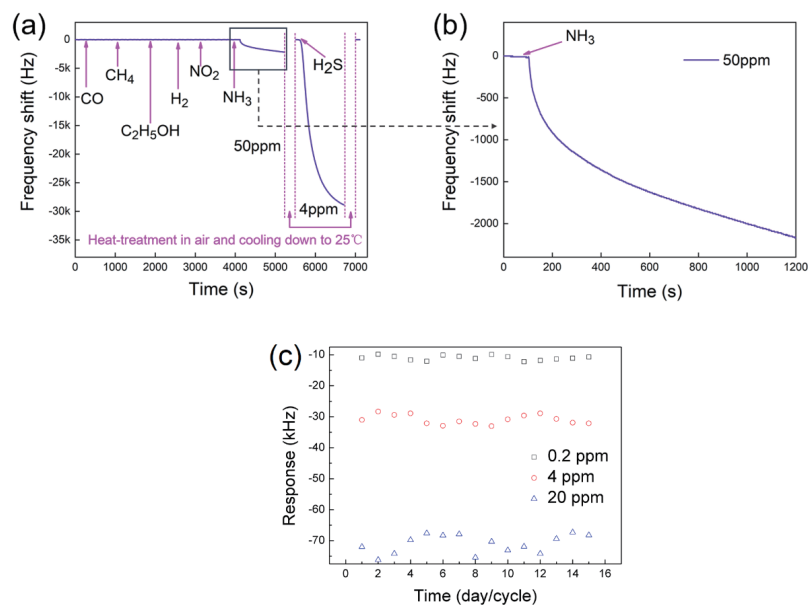
Fig. 9.   (Color online) (a) Responses of sensor to 100 ppm CO, CH_4, CH_3CH_2OH, H_2, and NO_2, 50 ppm NH_3, and 4 ppm H_2S. (b) Magnification of the black box in (a). (c) The sensor's response toward 0.2, 4 and 20 ppm H_2S for 15 response/recovery cycles in 15 days.
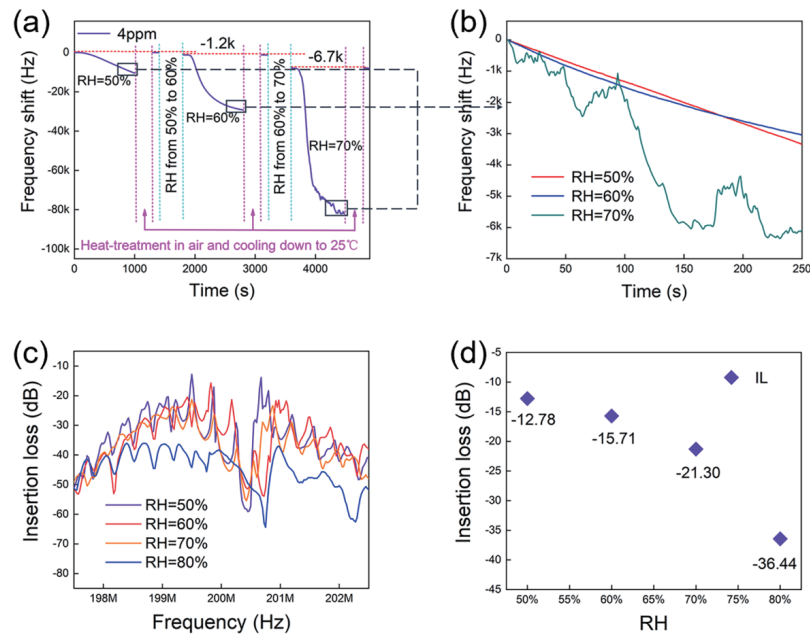
Fig. 10. (Color online) (a) Responses of sensor with Cu-20 to *RH* and H$_2$S at different *RH* values. (b) Magnified pictures in the black boxes in (a). (c) and (d) the transmission feature and insertion loss of the SAW resonator under different *RH* values.

4. Conclusions

In this study, we utilized a method that combined electron beam evaporation and annealing to deposit a CuO film on a two-port quartz SAW resonator, which was connected to peripheral circuits to build a highly sensitive and selective SAW H$_2$S sensor. EDS and Raman results revealed that the CuO can adsorb and react with H$_2$S to form CuS, which causes changes in the conductivity, elastic modulus, and mass of the film. In addition, the change in mass was found to be responsible for the negative frequency response of the sensor. With the increase in the thickness, the CuO film became rougher and presented more sites for the adsorption of H$_2$S, leading to the stronger responses of the sensors. However, the thicker film also led to higher noise of the sensor, which resulted in the highest SNR of the sensor with the thinnest CuO film. Humidity was found to strongly affect the sensing performance of the sensor, and higher *RH* values caused much stronger responses, whereas the noise level of the sensor also increased.

Conflicts of Interest

The authors declare no competing financial interest.

References

1 D. H. Truong, M. A. Eghbal, W. Hindmarsh, S. H. Roth, and P. J. O'Brien: Drug Metab. Rev. **38** (2006) 733. https://doi.org/10.1080/03602530600959607
2 E. Mansouri, J. Karamdel, M. Berahman, and M. T. Ahmadi: Phys. Status Solidi A **216** (2019) 1800086. https://doi.org/10.1002/pssa.201800086
3 T. S. Carpenter, S. M. Rosolina, and Z. L. Xue: Sens. Actuators, B **253** (2017) 846. https://doi.org/10.1016/j.snb.2017.06.114
4 P. Haouzi, T. Sonobe, and A. Judenherc-Haouzi: Ann. N. Y. Acad. Sci. **1374** (2016) 29. https://doi.org/10.1111/nyas.13015
5 A. Saeedi, A. Najibi, and A. Mohammadi-Bardbori: Int. J. Occup. Env. Med. **6** (2015) 20. https://doi.org/10.15171%2Fijoem.2015.482
6 T. L. Guidotti: Int. J. Toxicol. **29** (2010) 569. https://doi.org/10.1177/1091581810384882
7 J. M. Mir, R. C. Maurya, and M. W. Khan: Rev. Inorg. Chem. **42** (2022) 179. https://doi.org/10.1515/revic-2021-0009
8 K. H. Kim, E. C. Jeon, Y. J. Choi, and Y. S. Koo: Atmos. Environ. **40** (2006) 4478. https://doi.org/10.1016/j.atmosenv.2006.04.026
9 I. Iliuta and F. Larachi: Chem. Eng. Sci. **58** (2003) 5305. https://doi.org/10.1016/j.ces.2003.09.009
10 M. M. Asad, R. B. Hassan, F. Sherwani, Q. M. Soomro, S. Sohu, and M. T. Lakhiar: 2019 2nd Int. Conf. Computing, Mathematics and Engineering Technologies (iCoMET, 2019) IEEE. https://doi.org/10.1109/ICOMET.2019.8673516
11 Z. Li, Y. Huang, S. Zhang, W. Chen, Z. Kuang, D. Ao, and Y. Fu: J. Haz. Mat. **300** (2015) 167. https://doi.org/10.1016/j.jhazmat.2015.07.003
12 C. Yu, Y. Wang, K. Hua, W. Xing, and T. Lu: Sens. Actuators, B **86** (2002) 259. https://doi.org/10.1016/S0925-4005(02)00200-9
13 M. M. Choi and P. Hawkins: Sens. Actuators, B **90** (2003) 211. https://doi.org/10.1016/S0925-4005(03)00030-3
14 L. Rana, R. Gupta, M. Tomar, and V. Gupta: Sens. Actuators, B **252** (2017) 840. https://doi.org/10.1016/j.snb.2017.06.075
15 J. Che, J. S. Wang, C. C. Qiao, Y. D. Xia, K. Ou, J. Zhou, Y. X. Ni, W. T. Zhang, Y. C. Han, X. T. Zu, Y. Q. Fu, and Y. L. Tang: Sen. Actuators, A **353** (2023) 114225. https://doi.org/10.1016/j.sna.2023.114225
16 Y. L. Tang, X. F. Xu, S. B. Han, C. Cai, H. R. Du, H. Zhu, X. T. Zu, and Y. Q. Fu: Sens. Actuators, B **304** (2020) 127395. https://doi.org/10.1016/j.snb.2019.127395
17 C. Wang, L. J. Wang, L. Zhang, R. Xi, H. Huang, S. H. Zhang, and G. B. Pan: J. Alloy. Compd. **790** (2019) 363. https://doi.org/10.1016/j.jallcom.2019.03.084
18 M. Punginsang, D. Zappa, E. Comini, A. Wisitsoraat, G. Sberveglieri, A. Ponzoni, and C. Liewhiran: Appl. Surf. Sci. **571** (2022) 151262. https://doi.org/10.1016/j.apsusc.2021.151262
19 P. G. Su and Y. T. Peng: Sens. Actuators, B **193** (2014) 637. https://doi.org/10.1016/j.snb.2013.12.027
20 W. Luo, J. Deng, Q. Fu, D. Zhou, Y. Hu, S. Gong, and Z. Zheng: Sens. Actuators, B **217** (2015) 119. https://doi.org/10.1016/j.snb.2014.10.078
21 J. S. Wang, J. Che, C. C. Qiao, B. Niu, W. T. Zhang, Y. C. Han, Y. Q. Fu, and Y. L. Tang: Sens. Actuators, B **367** (2022) 132160. https://doi.org/10.1016/j.snb.2022.132160
22 D. J. Li, Y. L. Tang, D. Y. Ao, X. Xiang, S. Y. Wang, and X. T. Zu: Int. J. Hydrogen Energy **44** (2019) 3985. https://doi.org/10.1016/j.ijhydene.2018.12.083
23 D. J. Li, X. T. Zu, D. Y. Ao, Q. B. Tang, Y. Q. Fu, and Y. J. Guo: Sens. Actuators, B **294** (2019) 55. https://doi.org/10.1016/j.snb.2019.04.010
24 K. Sahu, R. Singhal, and S. Mohapatra: Catal. Lett. **150** (2020) 471. https://doi.org/10.1007/s10562-019-03009-w
25 T. H. Tran, M. H. Nguyen, T. H. T. Nguyen, V. P. T. Dao, Q. H. Nguyen, C. D. Sai, and V. T. Nguyen: Appl. Surf. Sci. **509** (2020) 145325. https://doi.org/10.1016/j.apsusc.2020.145325
26 H. T. Nha, P. Van Tong, N. Van Duy, C. M. Hung, and N. D. Hoa: J. Electron. Mater. **50** (2021) 2767. https://doi.org/10.1007/s11664-021-08799-7
27 S. Kamimura, N. Beppu, Y. Sasaki, T. Tsubota, and T. Ohno: J. Mater. Chem. A **5** (2017) 10450. https://doi.org/10.1039/C7TA02740K

28   A. G. Milekhin, N. A. Yeryukov, L. L. Sveshnikova, T. A. Duda, E. E. Rodyakina, V. A. Gridchin, and D. R. Zahn: Beilstein J. Nanotech. **6** (2015) 749. https://doi.org/10.3762/bjnano.6.77

29   S. S. Dhasade, J. S. Patil, J. H. Kim, S. H. Han, M. C. Rath, and V. J. Fulari: Mater. Chem. Phys. **137** (2012) 353. https://doi.org/10.1016/j.matchemphys.2012.09.033

30   A. J. Ricco, S. J. Martin, and T. E. Zipperian: Sens. Actuators **8** (1985) 319. https://doi.org/10.1016/0250-6874(85)80031-7

31   S. Arora, K. Kabra, K. B. Joshi, B. K. Sharma, and G. Sharma: Physica B **582** (2020) 311142. https://doi.org/10.1016/j.physb.2018.11.007

32   D. S. Ballantine Jr, S. J. Martin, A. J. Ricco, G. C. Frye, H. Wohltjen, R. M. White, and E. T. Zellers: Acoustic Wave Sensors: Theory, Design, and Physico-Chemical Applications (Academic Press, San Diego, 1997).